arXiv:2210.17145v2 [stat.ML] 8 Oct 2023

PROBABILITY-DEPENDENT GRADIENT DECAY IN LARGE MARGIN SOFTMAX

Siyuan Zhang
School of Internet of Things Engineering
Jiangnan University
Wuxi, China
6191905048@stu.jiangnan.edu.cn

Linbo Xie
School of Internet of Things Engineering
Jiangnan University
Wuxi, China
xie_linbo@jiangnan.edu.cn

Ying Chen
Key Laboratory of Advanced Process Control for Light Industry (Ministry of Education)
Jiangnan University
Wuxi, China
chenying@jiangnan.edu.cn

ABSTRACT

In this paper, a gradient decay hyperparameter is introduced in Softmax to control the probability-dependent gradient decay rate. By following the theoretical analysis and empirical results, we find that the generalization and calibration depend significantly on the gradient decay rate as the confidence probability rises, i.e., the gradient decreases convexly or concavely as the sample probability increases. Moreover, optimization with the small gradient decay shows a curriculum learning sequence where hard samples are in the spotlight only after easy samples are convinced sufficiently, and well-separated samples gain a higher gradient to reduce intra-class distance. Unfortunately, the small gradient decay exacerbates model overconfidence, shedding light on the causes of the poor calibration observed in modern neural networks. Conversely, a large gradient decay significantly mitigates these issues, outperforming even the model employing post-calibration methods. Based on the analysis results, we can provide evidence that the large margin Softmax will affect the local Lipschitz constraint by regulating the probability-dependent gradient decay rate. This paper provides a new perspective and understanding of the relationship among large margin Softmax, curriculum learning and model calibration by analyzing the gradient decay rate. Besides, we propose a warm-up strategy to dynamically adjust gradient decay.

Keywords Gradient decay · Large margin Softmax · Local Lipschitz constraint · Curriculum learning · Model calibration

1 Introduction

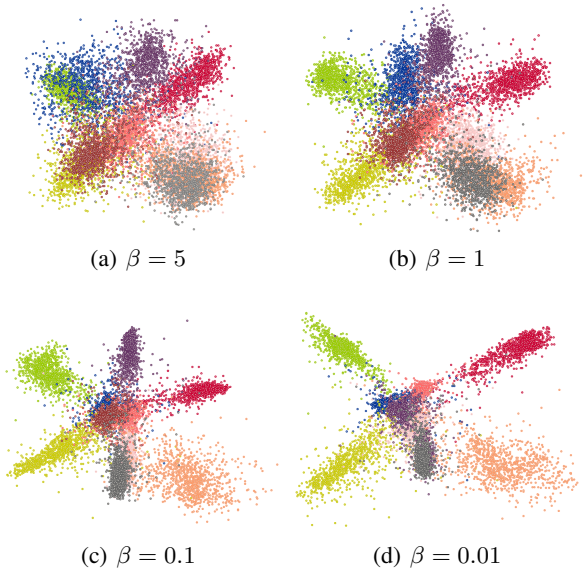
Softmax function combined with a cross-entropy loss (CE) as the logically reasonable loss function in empirical risk minimization of classification, has been recognized as the state-of-the-art base objective function in practical neural network optimization. Compared to the base regression criterion MSE (Mean Square Error), it is demonstrated in [1] that CE has a faster convergence rate since MSE takes into account more complex optimization scenarios. Softmax function converts the whole output space into an approximate probability distribution as a measure of the distance between the predicted distribution and the label. An important characteristic worth highlighting is that even in cases where continuous learning leads to minor training errors, it can still improve the implicit regularization of the network in classification with CE [2]. Similarly, all samples become support vectors when the model with CE keeps long-standing training in the over-parameterized model [3].

The Softmax function is usually defined by a single hyperparameter, the temperature τ,which scales the smoothness between Softmax and max function. The temperature τ is often discussed in contractive learning [4], knowledge distilling [5], natural language processing [6] and so on. In some specific tasks, the default Softmax is unable to learn discriminative features sufficiently. A small preset temperature τ can produce a hefty penalty on hard negative samples to force more significant inter-class discrepancy. Moreover, the penalty distribution tends to be more uniform as the temperature increases [7]. It seems reasonable that static model calibration plays the pivotal role [8]. Nevertheless, the literature [9] demonstrates that the dependence of the generalization on temperature is due to a dynamical phenomenon rather than model confidence.

Similarly, the hard mining strategy explicitly emphasizes more challenging samples by discarding easy samples or enlarging the weights of false negative samples that will benefit training [10, 11]. Based on the loss values, mining-based Softmax concentrates on the informative samples, so can learn more discriminative features [12, 13]. Selecting the value sample and removing noisy data are the technical foundation of the hard mining strategy. On the other hand, a soft mining strategy, like focal loss, smooths the mining strategy by introducing a modifiable hyperparameter so that the hard sample can be given more importance [14]. Due to its broad applicability, it has become a prevailing loss [15].

Another branch of Softmax research is the large margin Softmax, which increases the feature margin from the perspective of the ground truth class. Liu et al. introduced Large-margin Softmax (L-Softmax) [16] and Angular Softmax (A-Softmax) [17] to impose discriminative constraints on a hypersphere manifold to encourage intra-class compactness and inter-class separability between learned features. Wang et al. proposed a more interpretable way to import the angular margin into Additive Margin Softmax (AM-Softmax) [18]. In [19], the Additive Angular Margin Loss (ArcFace) showed a clear geometric interpretation due to its exact correspondence to geodesic distance on a hypersphere. Unlike the hard mining strategy, large margin Softmax not only swells the inter-class distance by adjusting the temperature but also remains focused on the intra-class distance. However, to the best of our knowledge, there is a lack of corresponding explanatory work from dynamic training performance. Our findings will demonstrate that the "margin" could contribute to overconfidence in over-parameterized models.

This paper introduces a hyperparameter β in Softmax, which controls the probability-dependent gradient decay as the sample confidence probability rises. From the theoretical analysis, we can conclude that the smaller the hyperparameter β is, the smoother the local L-constraint of the Softmax is. It means that the model with a smaller β can obtain a rapider convergence rate in the initial phase. As shown in Fig. 1, minor gradient decay produces a higher gradient to the well-separated sample to shrink the intra-class distance at the expense of "discarding" some hard negative samples due to the limited network capacity. The training with a slight gradient decay shows a similar curriculum learning idea [20, 21, 22] that the hard samples will be optimized only after the easy samples have been convinced sufficiently. Unfortunately, small probabilistic gradient decays worsen the miscalibration of the modern model, while larger decay rates generally smooth the training sequence, alleviating this issue. This paper analyzes the dynamic training phenomenon with different β and provides a new understanding of large margin Softmax by considering the effect of the hyperparameters β on gradient decay rate. Besides, we propose a warm-up training strategy to set an over-small initial hyperparameter β to speed up the convergence rate. Then, β is enlarged to an adequate value to prevent over-confidence.



(a) $\beta = 5$ (b) $\beta = 1$ (c) $\beta = 0.1$ (d) $\beta = 0.01$

Figure 1: The features distribution with different gradient decay factors.

2 Preliminaries

In classification, the class label can be predicted using the one-versus-all technique as

$$cls\left(z\left(x\right)\right) = \max\left\{z_i\left(x\right)\right\}, i = 1, \ldots, m \tag{1}$$

where $z_i, i = 1, \ldots, m$ represent the outputs of m labels. c represents the truth class in m classes. Logically, we hope the output z_c can be larger than other class outputs $z_i, i = 1, \ldots, m, i \neq c$.

$$\arg\min z_i - z_c, i = 1, \ldots, m, i \neq c \tag{2}$$

To smooth the above $m - 1$ optimization problems in (2), we can obtain a logically equivalent objective for the above problem. That is, minimizing the output of the category most adversarial to z_c.

$$\arg\min \max\{z_i - z_c\}, i = 1, \ldots, m, i \neq c \tag{3}$$

Then, two hyperparameters are introduced into (3), temperature τ and margin $\log \beta$, where $\beta > 0$.

$$\arg\min \max \left\{\log \beta, z_i - z_c/\tau\right\}, i = 1, \ldots, m, i \neq c \tag{4}$$

Although the max function is convex, it is discrete and (4) is hard to optimize by gradient descent. So, (4) needs to be smoothed by sum-exp-up (also called Softmax), as follows:

$$\begin{aligned} &\max \left\{\log \beta, z_i - z_c/\tau\right\}, i = 1, \ldots, m, i \neq c \\ &\approx \log \textstyle\sum_{i \neq c} e^{z_i - z_c/\tau} + \beta \\ &= -\log \frac{e^{z_c/\tau}}{\sum_{i \neq c} e^{z_i/\tau} + \beta e^{z_c/\tau}} \end{aligned} \tag{5}$$

The temperature τ in (5) has been widely researched in the literature [4] and the reference therein.

$$\lim_{\tau \to 0} -\log \frac{e^{z_c/\tau}}{\sum e^{z_i/\tau}} = \lim_{\tau \to 0} \max \left\{z_i - z_c/\tau\right\}, i = 1, \ldots, m \tag{6}$$

When τ approaches 0, the cross entropy is approximated as a max function of the difference between the truth class output and other class outputs. The model will pay more attention to the hard negative sample near the decision boundary so that the inter-class can be scattered. Larger τ means that the model will handle all class outputs of the sample more smoothly. Some papers attribute the improvement of the temperature scaling solely to the calibration of the model confidence [4]. A challenge was raised in [9] that the dependence of the generalization on temperature is due to a dynamical phenomenon rather than model confidence.

In (4), the hyperparameter β represents the soft margin in decision space. So the cross-entropy itself can be interpreted as a margin-based loss [14]. However, the above large margin is defined in the features of the output space. Owing to the distance distortion between input and representation spaces, the large margin in the input space of models is not maximized simultaneously by large margin Softmax. Margin within the input space plays a more substantial role in generalization and robustness. That is reflected that a more considerable margin does not mean better generalization. Besides, the margins defined based on different criteria realize different performances, i.e., angular margin or cosine margin. So the interpretation of its effect is slightly ambiguous.

On the other hand, the model training is associated with $J_j, j = 1, \ldots, n$, which n represents sample number, and n optimization problems are equally combined as a multi-objective optimization $\sum_{j=1}^{n} J_j$. The coupling effect among the samples should be considered in the dynamic optimization process.

3 GRADIENT DECAY

3.1 Gradient decay hyperparameter

We consider the Softmax with the sole hyperparameter β. The temperature τ is set to 1.

$$J = -\log \frac{e^{z_c}}{\sum_{i \neq c} e^{z_i} + \beta e^{z_c}} \tag{7}$$

Let us first consider the gradient of the Softmax.

$$\frac{\partial J}{\partial z_c} = -\frac{\sum e^{z_i} - e^{z_c}}{\sum e^{z_i} + (\beta - 1) e^{z_c}} \tag{8}$$

$$\frac{\partial J}{\partial z_i} = \frac{e^{z_i}}{\sum e^{z_i} + (\beta - 1) e^{z_c}} \tag{9}$$

We introduce probabilistic output $p_i = \frac{e^{z_i}}{e^{z_1} + \cdots + e^{z_m}}$ as an intermediate variable. Then we obtain:

$$\frac{\partial J}{\partial z_i} = \begin{cases} -\dfrac{1 - p_c}{1 + (\beta - 1) p_c}, i = c \\ \dfrac{p_i}{1 + (\beta - 1) p_c}, i \neq c \end{cases} \tag{10}$$

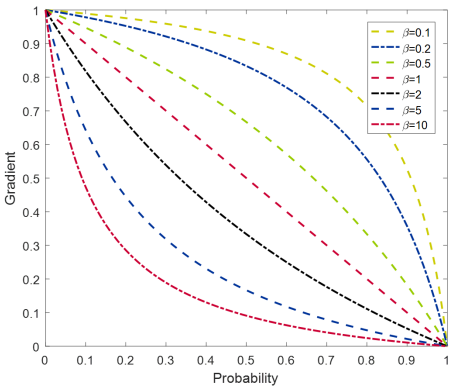


Figure 2: The gradient magnitude.

Since $\left|\frac{\partial J}{\partial z_c}\right| + \sum_{i \neq c}\left|\frac{\partial J}{\partial z_i}\right| = 2\left|\frac{\partial J}{\partial z_c}\right|, \left|\frac{\partial J}{\partial z_c}\right|$ can represent the gradient magnitude of this sample. Moreover, p_c can represent the confidence of the model for this sample. In (10), we can conclude that β determines the gradient magnitude related to sample probability confidence. We define the gradient magnitude $G = -\frac{\partial J}{\partial z_c}$. Then, we can get first-order and second-order derivatives of G with respect to p_c.

$$\frac{\partial G}{\partial p_c} = \frac{-\beta}{\left(1 + (\beta - 1)p_c\right)^2} \tag{11}$$

$$\frac{\partial^2 G}{\partial {p_c}^2} = \frac{2\beta(\beta - 1)}{\left(1 + (\beta - 1)p_c\right)^3} \tag{12}$$

When $\beta > 1$, $\frac{\partial^2 G}{\partial {p_c}^2} > 0$, gradient magnitude decreases concave monotonically as the sample probability rises; When $1 > \beta > 0$, $\frac{\partial^2 G}{\partial {p_c}^2} < 0$, gradient magnitude shows convex monotonically decreasing as the sample probability rises. As shown in Fig. 2, β controls the gradient decay rate as the sample probability rises. The smaller hyperparameter β shows a lower gradient decay rate in the initial phase. Furthermore, the gradient magnitude decays rapidly after the probability exceeds a certain value, which can be interpreted as a soft probability margin.

However, derivatives of G to p_c seem to be abstract. So, we need to obtain the second-order and the third-order derivatives of J to the truth class output z_c. We introduce the intermediate variable p_c.

$$\frac{\partial^2 J}{\partial {z_c}^2} = \frac{\partial^2 J}{\partial z_c \partial p_c}\frac{\partial p_c}{\partial z_c} \tag{13}$$

Because $\frac{\partial p_c}{\partial z_c} = p_c\left(1 - p_c\right)$. So we get $\frac{\partial^2 J}{\partial {z_c}^2} = \frac{\beta p_c(1-p_c)}{(1+(\beta-1)p_c)^2}$ and

$$\frac{\partial^3 J}{\partial {z_c}^3} = \frac{\beta p_c\left(1 - p_c\right)}{\left(1 + (\beta - 1)p_c\right)^3}\left(1 - (1 + \beta)\, p_c\right) \tag{14}$$

$\frac{\beta p_c(1-p_c)}{(1+(\beta-1)p_c)^3} > 0$ is constant since $\beta > 0$ and $1 > p_c > 0$. So $\frac{\partial^3 J}{\partial {z_c}^3} < 0$ when $p_c > \frac{1}{1+\beta}$; $\frac{\partial^3 J}{\partial {z_c}^3} > 0$ when $p_c < \frac{1}{1+\beta}$. We concentrate on the change of the gradient magnitude G. Thus, the magnitude shows convex monotonically decreasing as z_c increases when $p_c < \frac{1}{1+\beta}$, and concave monotonically decreasing when $p_c > \frac{1}{1+\beta}$. $p_c = \frac{1}{1+\beta}$ is the inflection point of gradient as the z_c increases. β determines the inflection point.

The magnitude of the gradient always decays from 1 to 0. As shown in Fig. 2, smaller β produces a smoother decay in the initial phase, which results in a larger magnitude in the whole training. The inflection gradually moves away from the initial point $z_c = 0$ so that a smooth gradient and large magnitude can dominate training, as shown in Fig. 7. So, a small hyperparameter β induces a low gradient decay rate and large gradient magnitude.

Let us consider two extreme cases: $\beta \to 0^+$ and $\beta \to +\infty$.

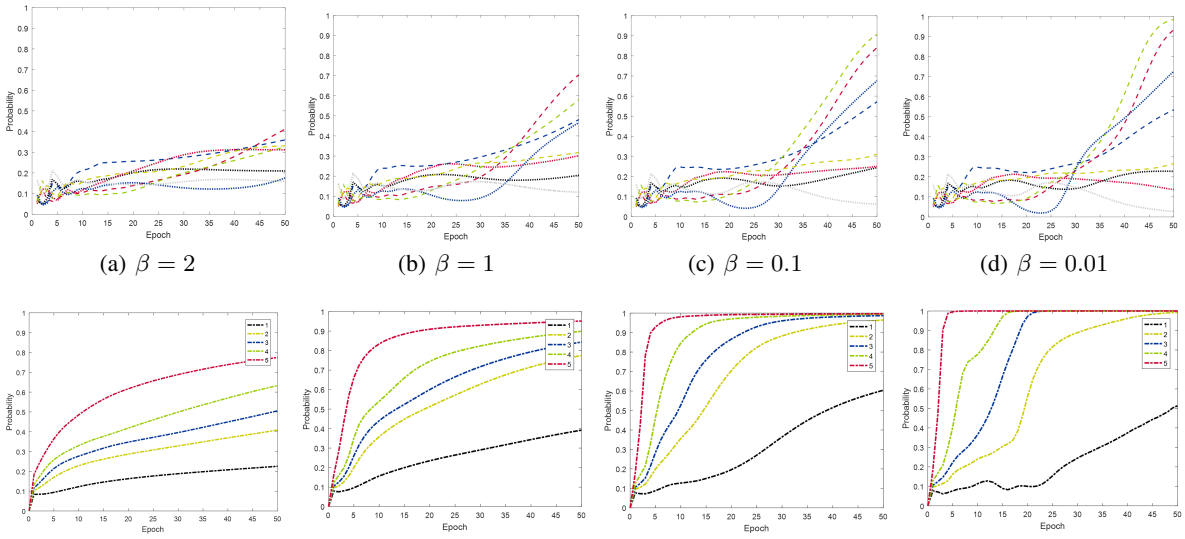
$$\lim_{\beta \to 0^+} G = \lim_{\beta \to 0^+} \frac{1 - p_c}{1 + (\beta - 1)p_c} = 1 \tag{15}$$

$$\lim_{\beta \to +\infty} G = \lim_{\beta \to +\infty} \frac{1 - p_c}{1 + (\beta - 1)p_c} = 0 \tag{16}$$

Obviously, $\beta \to 0^+$ will keep the sum of the gradient amplitudes $\left|\frac{\partial J}{\partial z_c}\right| + \sum_{i \neq c}\left|\frac{\partial J}{\partial z_i}\right|$ unchanged. In Fig. 2, the curve will be approximated as a step function where $G = 1, p_c < 1$ and $G = 0, p_c = 1$. On the other hand, $\beta \to +\infty$ forces the gradient down rapidly to 0. It is reflected in the changes of the convexity of the curves and the panning of the inflection point.

3.2 How does the gradient decay rate affect the model performance?

Fast gradient decay produces a slight gradient in the early phase of optimization. So the training may be prone to trap into local minima before sufficient learning in the early training phase. From the perspective of dynamic multi-objective



(a) $\beta = 2$ (b) $\beta = 1$ (c) $\beta = 0.1$ (d) $\beta = 0.01$

(e) $\beta = 2$ (f) $\beta = 1$ (g) $\beta = 0.1$ (h) $\beta = 0.01$

Figure 3: Dynamic confidence during training of MNIST. Top row a-d: Confidence of some samples during training. Bottom row e-h: Mean confidence of five groups of samples during training.

Table 1: Confidence distribution of the samples with different gradient decay factors on MNIST. # indicates the number of samples that belong to the confidence interval.

Gradient decay factor β	1	0.5	0.1	0.01	0.001
$\#p_c \leq 0.2$	903	828	1105	1325	2375
$\#0.2 < p_c \leq 0.4$	454	206	119	91	142
$\#0.4 < p_c \leq 0.6$	528	245	132	92	116
$\#0.6 < p_c \leq 0.8$	1291	484	191	100	193
$\#0.8 < p_c \leq 1$	56824	58237	58453	58392	57174

optimization $\sum_{j=1}^{n} J_j$, hard objectives can always chase the easy objectives and stay consistent with the easy objectives in optimization due to the large probability-dependent gradient decay, as shown in Fig. 3. The gradient of well-separated sample is forced to decrease rapidly. A more significant constraint exists on the synchronization of the optimization process for different samples. Consequently, there is a lack of distinction between samples, potentially leading to model under-confidence.

A gradual decrease in gradient magnitude consistently prioritizes well-separated samples during training. The influence of easy samples persists until reaching the predefined margin, after which gradients gradually decline. Consequently, well-separated samples receive ample attention and output feature can be gathered more compactly, as shown in Fig. 1. Then the intra-class variance can be shrunk and discriminative features can be learned by the higher gradient [23].

Furthermore, the low gradient decay training strategy is similar to curriculum learning. That is, the samples should be learned strictly sequentially from easy to hard. In traditional curriculum learning, the samples usually are labeled as "easy" or "hard" by complicated offline or online strategies [24]. A smooth gradient implicitly ensures the strict training sequence and softly divides the sample optimization by posterior probability. As shown in Fig. 3, the optimization of the prevailing Softmax with $\beta = 1$ keeps relatively consistent, while the smaller β shows distinguishability over different samples. Figs. 3e-h show the mean confidence of the different sample groups with different gradient decay rates. The classes "1-5" represent the five sample classes from "hard" to "easy". The default Softmax with $\beta = 1$ is relatively conservative for the sample training, while the Softmax with smaller gradient decay is more inclined to mine more information in easy samples under a soft curriculum idea. It can be inferred that the smaller gradient decay can realize the stricter curriculum sequence. Moreover, small gradient decay usually performs better convergence rate, but too low gradient decay does not imply better results. As shown in section 4.2, small gradient decay may result in worse miscalibration of the over-parameterized model, while larger decay rates generally smooth the training sequence, thus alleviating this issue.

Gradually reducing the gradient decay facilitates effective learning of discriminative features. From the comparison between Fig. 3f and Fig. 3g, the probability can be enlarged for almost all samples. In the practical application, the slight boost is very important to improve generalization and robustness, although the error is very small [2]. However, the network capacity is limited and there is no free lunch [25]. If we make excessive demands on the margin, some post-training samples cannot get any chance and will be "sacrificed" according to the soft curriculum learning strategy, as shown in grey curve of Fig. 3c and Fig. 3d. The result in Tab. 1 shows that the number of the samples with low confidence $\#p_c \leq 0.2$ increases as β is set to an over-small value. The over-large margin in [18] will discard some hard negative samples under limited model capacity, since the model gives more priority to easy samples. The intra-class distance of the partial positive easy samples will be reduced at the expense of the inter-class distance of some hard negative samples near the decision boundary. So there is a clear difference between the large margin Softmax and hard mining strategies: the former focuses on the overall confidence or even more on the mining of easy samples while the latter focuses more on hard samples.

Confidence calibration between τ and β : The Softmax with small τ disperses the inter-class distance by adjusting the probability output to focus more on hard negative samples. Nevertheless, large τ can only smooth the output of all categories and cannot mine more information from simple positive samples. On the contrary, small β makes the gradient decay slowly so that easy positive samples can be sufficiently learned up to high confidence as shown in Fig. 3. An appropriate β can mining more discriminative features on the whole. Similarly, large β only keeps the consistency of the overall sample training and cannot extract more meaningful features from challenging samples.

In terms of the training process, τ changes the probability distribution of the class outputs and β determines the gradient magnitude assigned by the probability of belonging to the truth class. They improved the mining capability of Softmax in two different dimensions. So it is convinced that the general Softmax loss should be defined with these two hyperparameters τ and β.

3.3 Local Lipschitz constraint

Assume that the gradient of the function $J(\mathrm{z})$ satisfies Lipschitz constraint (L-constraint) that is

$$\left\|\nabla_z J(z+\Delta z)-\nabla_z J(z)\right\|_2 \leq L\|\Delta z\|_2 \tag{17}$$

For a second-order differentiable objective function, the above condition is equivalent to $\left\|\nabla_z^2 J(z)\right\|_2 \leq L$, where L represents the degree of fluctuation of the gradient. Then we have the following inequality [26].

$$J(z+\Delta z) \leq J(z)+\langle\nabla_z J(z), \Delta z\rangle+\frac{1}{2} L\|\Delta z\|_2^2 \tag{18}$$

The gradient descent is applied to optimization. $\Delta z=-\eta \nabla_z J(z)$, where $\eta>0$ is the learning rate. Substituting it into (18), we obtain

$$J(z+\Delta z) \leq J(z)+\left(\frac{1}{2} L \eta^2-\eta\right)\left\|\nabla_z J(z)\right\|_2^2 \tag{19}$$

So, $\frac{1}{2} L \eta^2-\eta<0$ is the sufficient condition for loss decline at each iteration. And $\frac{1}{2} L \eta^2-\eta$ is the minimum value when $\eta^*=\frac{1}{L}$. The larger the magnitude of the gradient $\left\|\nabla_z J(z)\right\|_2^2$ is, the smaller the L-constraint is. Furthermore, the smaller L-constraint results in the rapider convergence [26]. The learning rate η can be adaptively designed to maximize the convergence speed [27]. Unfortunately, L-constraint is an intrinsic property of the loss function.

Since $\left|\frac{\partial J}{\partial z_c}\right|=\sum_{i \neq c}\left|\frac{\partial J}{\partial z_i}\right|$, we consider the only variable z_c in Softmax. For function $J(z_c)$ as shown in (11-14), we obtain that the $\max \left\|\nabla_{z_c}^2 J(z_c)\right\|_2$ is $\frac{1}{4}$ when $p_c=\frac{1}{1+\beta}$. So β cannot change the global L-constrain since it is a constant. However, the local L-constrain can be adjusted by overall panning. Thus, we can narrow β and change the inflection point of the gradient $p_c=\frac{1}{1+\beta}$ so that the constant maximum is far from the initial point, allowing a larger range of the smooth gradient to occupy the optimization process. For example, we consider the local range $p_c \in[0,0.5]$ and can obtain a local L-constrain of $\left\|\nabla_{z_c}^2 J(z_c)\right\|_2$ as follows:

$$\begin{cases}\left\|\nabla_{z_c}^2 J(z_c)\right\|_2 \leq \dfrac{\beta}{(\beta+1)^2}, \beta<1 \\ \left\|\nabla_{z_c}^2 J(z_c)\right\|_2 \leq \dfrac{1}{4} \qquad\quad , \beta \geq 1\end{cases} \tag{20}$$

So it can be demonstrated that the β smaller is, the gradient smoother is. When β is set to a small value, the learning rate η of gradient descent in (20) can be amplified to accelerate the optimization. On the other hand, the gradient magnitude $\|\nabla_{z_c} J(z_c)\|_2^2$ of smaller β is always greater than that of larger β. Besides, it is meaningful that we can change β to control the local L-constraint of the Softmax loss in optimization. Some literature [28] have shown that the Lipschitz constraint of the gradient has been strongly related to model generalization and robustness. The regularization of the gradient L-constraint has been applied to obtain the large margin decision boundary or guarantee the stable optimization in Generative Adversarial Networks (GAN) [29].

3.4 Warm-up strategy

Based on the above analysis, we can conclude that the smaller β produces a larger gradient magnitude with less gradient decay in the initial phase and can realize faster convergence. However, some hard negative samples may be discarded by over-small β. The risk of model overconfidence is exacerbated. Thus, we propose a warm-up training strategy, where over-small β in the initial phase provides fast convergence with the smooth local L-constraint and increases gradually until an adequate set. Then, easy sample can be learned sufficiently in early training and over-miscalibration of final model can be avoid. In this paper, we use a simple linear warm-up strategy as $\beta = \frac{\beta_{end}-\beta_{initial}}{t_{warm}} t + \beta_{initial}$, where $\beta_{initial}$ and β_{end} are preset initial and final values. t_{warm} and t represent the end iteration of warm-up strategy and current iteration, respectively. $\beta_{initial}$ gradually increases to preset β_{end} in the training.

4 EMPIRICAL VERIFICATION

4.1 Convergence rate and accuracy

It is shown in Fig. 4 that the performance of different gradient decays shows different phenomena. The Softmax with less gradient decay displays faster convergence and better generalization with discriminate feature learning. $\beta = 0.01$ realizes the better accuracy than traditional CE with $\beta = 1$ and the large gradient decay has worse performance .

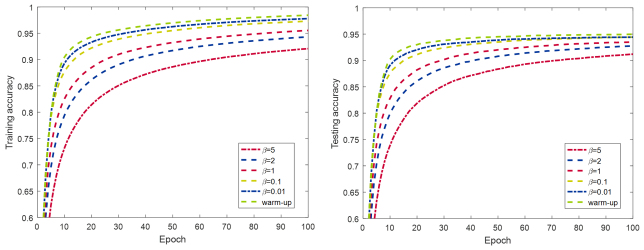


Figure 4: The performance on MNIST.

The warm-up strategy sets a small initial gradient decay hyperparameter β to speed up the convergence rate and guarantees final stable performance by increasing β to prevent over-confidence for easy sample. Warm-up strategy achieves even better results. Furthermore, decline curves of cross-entropy loss with different β are shown in Fig. 5 to empirically show the high convergence rate of small gradient decay. It can be inferred that minor gradient decay shows the rapider convergence rate, although the gap decreases due to the deviation between the general cross-entropy loss and objective functions with different β. Significantly, the result of this experiment is enough to empirically show that minor gradient decay with small L-constraint can achieve a faster convergence rate.

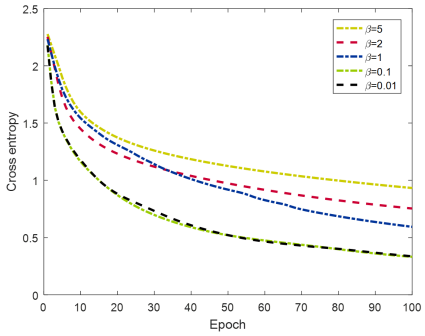


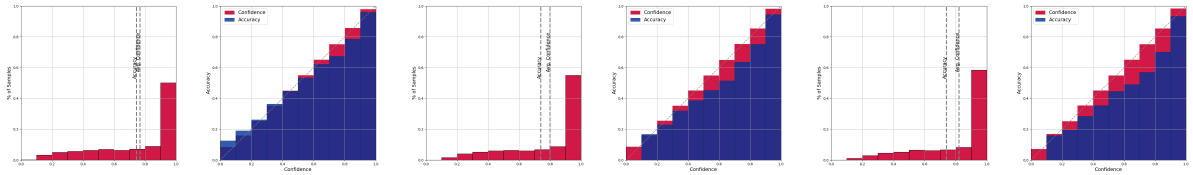
Figure 5: CE with different gradient decay.

The top-1 accuracy of several deep models are given in Tab. 2. It can be concluded that top-1 accuracy of these models benefit from the more minor gradient decay in SVHN and CIFAR-10. However, over-small gradient decay pursuits the smaller intra-class distance under the limited capacity of the network. Some challenging samples cannot get enough training and may be discarded. So as shown in Tab. 2, the larger β cannot always indicate a better performance.

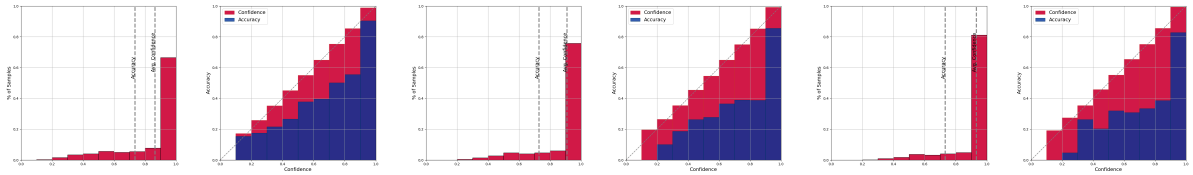
On the other hand, a large β induces a large gradient decay and a large L-constraint of Softmax, which means that gradient change is sharp and the training of easy samples and challenging samples is relatively consistent, as discussed in Fig. 3. As a result, a small gradient magnitude could lead to insufficient training, as demonstrated in Tab. 2. This could elucidate the subpar outcomes associated with large gradient decay coefficients in CIFAR-10 and SVHN datasets. A potential avenue for future

Table 2: Top-1 accuracy with different methods and gradient decay factors

Dataset	Model	Gradient decay factor β					Warm-up	A-Softmax	Center loss
		5	2	1	0.1	0.01			
SVHN	ResNet18	94.5	94.8	94.9	95.8	95.6	95.9	**96.0**	95.7
SVHN	ResNet35	95.0	95.2	95.5	96.1	96.0	**96.2**	96.1	95.8
SVHN	VGG16	95.1	95.3	95.4	**96.1**	95.8	96.0	95.9	95.7
SVHN	MobileNetV1	94.1	94.5	95.0	95.2	95.5	95.9	**96.2**	95.6
CIFAR-10	ResNet18	94.2	94.3	94.3	94.5	94.3	**94.9**	94.6	94.5
CIFAR-10	ResNet35	94.4	94.5	94.7	94.9	94.7	**95.2**	94.9	94.7
CIFAR-10	VGG16	92.9	93.2	93.0	93.4	93.2	93.7	**93.8**	93.6
CIFAR-10	MobileNetV1	93.0	93.1	93.0	**93.7**	93.5	**93.7**	93.5	**93.7**
CIFAR-100	ResNet18	74.1	73.6	73.5	73.2	72.8	**74.5**	73.3	73.6
CIFAR-100	ResNet35	74.5	74.0	74.0	73.8	73.4	**74.6**	73.6	73.9
CIFAR-100	VGG16	72.0	72.3	72.0	71.8	71.1	**72.5**	71.9	72.2
CIFAR-100	MobileNetV1	73.6	**73.9**	73.5	73.0	72.5	73.7	73.3	73.8
Tiny-ImageNet	ResNet34	53.8	53.7	53.4	53.7	53.6	54.0	**54.2**	52.9



(a) $\beta = 20$ (b) $\beta = 10$ (c) $\beta = 5$



(d) $\beta = 1$ (e) $\beta = 0.1$ (f) $\beta = 0.01$

Figure 6: Confidence and reliability diagrams with ResNet18 on CIFAR-100. ($bins = 10$)

research could involve dynamic adjustments of the training rate based on gradient decay to ensure sufficient and consistent training.

However, confidence is not always a good thing. Curriculum design that divides samples is crucial to curriculum learning idea. Apart from the manual design, most division can only be done by the posterior probability. When the model does not have enough capacity to solve a challenging task, confidence toward under-confident samples would damage the performance. Besides, based the previous analysis in section 3.2, small gradient decay rate may impair the performance since some hard negative samples containing important information are discarded. As shown in Tab. 2, these models on CIFAR-100 all prefer the large β. The difficulty of CIFAR-100 is reflected in more categories, which leads to a lower probability of true category. Since the smaller β keeps lower gradient decay in the low probability output, this experiment is more sensitive for small β. From another perspective, the mentioned model has no high probability confidence and the training material is not good enough. Learning every sample more equally is a better choice since the model cannot confidently determine which the simple sample is or which a more informative sample is by posterior probability. The large gradient decay [16, 17, 18] is a relative concept in different tasks.

4.2 Model calibration

To substantiate this conclusion on the model calibration, Fig. 6 displays the confidence histograms and reliability diagrams for different gradient descent factors on CIFAR-100 while Tab. 3 provides the ECE and MCE in different datasets, which are crucial metrics for assessing model calibration [7]. The results reveal that small decay coefficients,

Table 3: Model calibration of different gradient decay and post-processing calibration. ($bins = 10$)

Dataset	Model	Metric	Gradient decay factor β				Vector Scaling	Temp. Scaling
			20	10	1	0.1		
CIFAR-100	ResNet18	ECE	**0.021**	0.059	0.130	0.181	0.041	0.029
		MCE	**0.071**	0.135	0.298	0.464	0.152	0.076
CIFAR-100	ResNet34	ECE	**0.030**	0.065	0.125	0.170	0.037	0.031
		MCE	0.091	0.157	0.273	0.388	0.150	**0.049**
CIFAR-100	VGG16	ECE	0.131	0.177	0.212	0.233	0.028	**0.022**
		MCE	0.301	0.386	0.508	0.579	0.540	**0.044**
CIFAR-10	ResNet18	ECE	0.023	0.026	0.038	0.045	**0.012**	0.014
		MCE	0.728	0.291	0.286	0.379	**0.052**	0.097
Tiny-ImageNet	ResNet34	ECE	**0.015**	0.034	0.087	0.224	0.018	0.021
		MCE	**0.036**	0.065	0.176	0.406	0.038	0.068
Tiny-ImageNet	ResNet50	ECE	0.045	**0.014**	0.114	0.203	0.021	0.025
		MCE	0.084	0.044	0.151	0.388	**0.042**	0.073

corresponding to larger margin penalties in Softmax, result in overconfidence, rendering the probabilistic output less reliable. Conversely, a significant probability-dependent gradient decay mitigates model overconfidence.

Experimental results consistently demonstrate that as the gradient decay rate increases with rising probabilities, the average confidence also rises. This phenomenon can be attributed to the small gradient decay rate enforcing a strict curriculum learning sequence. The adjustment of probability-dependent gradient decay would significantly improve the confidence distribution in model training, surpassing some post-calibration methods even with rough tuning on CIFAR-100 and Tiny-ImageNet. We attribute the poor calibration to the small gradient decay rate, and this conclusion is compelling. More experimental results supporting this conclusion can be found in Appendix A.

5 Conclusion

This paper introduces the gradient decay hyperparameter β to analyze the effect of the large margin defined in decision space from a dynamical training process. The large margin of Softmax induces the small gradient decay as the sample probability rises. The easy positive samples can be learned sufficiently up to high probability and the model tends to be more confident toward these samples. Training displays distinguishability over different samples in training, i.e., the samples are optimized under the stricter curriculum sequence. Under the limited network capacity and over-large margin, reducing the intra-class distance of the partial easy positive samples will sacrifice the inter-class distance of hard negative samples. Empirical evidence demonstrates that small probabilistic gradient decays exacerbate the miscalibration of over-parameterized models. Conversely,increasing the gradient decay coefficient emerges as an effective strategy for alleviating issues related to overconfidence. Besides, the Softmax with smaller gradient decay has a smoother local L-constraint, so the large margin Softmax can obtain a faster convergence rate. Thus, we propose a warm-up training strategy to smoother L-constraint in early training and avoid over-confidence in final model.

References

[1] Pavel Golik, Patrick Doetsch, and Hermann Ney. Cross-entropy vs. squared error training: a theoretical and experimental comparison. In *INTERSPEECH*, 2013.

[2] Daniel Soudry, Elad Hoffer, Mor Shpigel Nacson, Suriya Gunasekar, and Nathan Srebro. The implicit bias of gradient descent on separable data. *Journal of Machine Learning Research*, 19(70):1–57, 2018.

[3] Roei Sarussi, Alon Brutzkus, and Amir Globerson. Towards understanding learning in neural networks with linear teachers. In *International Conference on Machine Learning (ICML)*, pages 9313–9322. PMLR, 2021.

[4] Feng Wang and Huaping Liu. Understanding the behaviour of contrastive loss. In *Proceedings of the IEEE/CVF Conference on Computer Vision and Pattern Recognition (CVPR)*, pages 2495–2504, June 2021.

[5] Geoffrey Hinton, Oriol Vinyals, Jeff Dean, et al. Distilling the knowledge in a neural network. *arXiv preprint arXiv:1503.02531*, 2(7), 2015.

[6] Pengfei Liu, Weizhe Yuan, Jinlan Fu, Zhengbao Jiang, Hiroaki Hayashi, and Graham Neubig. Pre-train, prompt, and predict: A systematic survey of prompting methods in natural language processing. *arXiv preprint arXiv:2107.13586*, 2021.

[7] Chuan Guo, Geoff Pleiss, Yu Sun, and Kilian Q Weinberger. On calibration of modern neural networks. In *International Conference on Machine Learning (ICML)*, pages 1321–1330. PMLR, 2017.

[8] Xu Zhang, Felix Xinnan Yu, Svebor Karaman, Wei Zhang, and Shih-Fu Chang. Heated-up softmax embedding. In *International Conference on Learning Representations (ICLR)*, 2018.

[9] Atish Agarwala, Jeffrey Pennington, Yann Dauphin, and S. Schoenholz. Temperature check: theory and practice for training models with softmax-cross-entropy losses. In *International Conference on Learning Representations (ICLR)*, 2020.

[10] Xiaobo Wang, Shifeng Zhang, Shuo Wang, Tianyu Fu, Hailin Shi, and Tao Mei. Mis-classified vector guided softmax loss for face recognition. In *Proceedings of the AAAI Conference on Artificial Intelligence (AAAI)*, pages 12241–12248, 2020.

[11] Yazhou Ren, Peng Zhao, Yongpan Sheng, Dezhong Yao, and Zenglin Xu. Robust softmax regression for multi-class classification with self-paced learning. In *International Joint Conference on Artificial Intelligence (IJCAI)*, pages 2641–2647, 2017.

[12] Abhinav Shrivastava, Abhinav Gupta, and Ross Girshick. Training region-based object detectors with online hard example mining. In *Proceedings of the IEEE/CVF Conference on Computer Vision and Pattern Recognition (CVPR)*, pages 761–769, 2016.

[13] Yuge Huang, Yuhan Wang, Ying Tai, Xiaoming Liu, Pengcheng Shen, Shaoxin Li, Jilin Li, and Feiyue Huang. Curricularface: adaptive curriculum learning loss for deep face recognition. In *proceedings of the IEEE/CVF Conference on Computer Vision and Pattern Recognition*, pages 5901–5910, 2020.

[14] W Zheng, J Lu, and J Zhou. Hardness-aware deep metric learning. *IEEE Transactions on Pattern Analysis and Machine Intelligence*, 43(9):3214–3228, 2021.

[15] Tsung-Yi Lin, Priya Goyal, Ross Girshick, Kaiming He, and Piotr Dollar. Focal loss for dense object detection. *IEEE Transactions on Pattern Analysis and Machine Intelligence*, 42(2):318–327, 2020.

[16] Weiyang Liu, Yandong Wen, Zhiding Yu, and Meng Yang. Large-margin softmax loss for convolutional neural networks. In *International Conference on Machine Learning (ICML)*, 2016.

[17] Weiyang Liu, Yandong Wen, Zhiding Yu, Ming Li, Bhiksha Raj, and Le Song. Sphereface: Deep hypersphere embedding for face recognition. In *Proceedings of the IEEE/CVF Conference on Computer Vision and Pattern Recognition (CVPR)*, pages 212–220, 2017.

[18] Feng Wang, Jian Cheng, Weiyang Liu, and Haijun Liu. Additive margin softmax for face verification. *IEEE Signal Processing Letters*, 25(7):926–930, 2018.

[19] Jiankang Deng, Jia Guo, Niannan Xue, and Stefanos Zafeiriou. Arcface: Additive angular margin loss for deep face recognition. In *Proceedings of the IEEE/CVF Conference on Computer Vision and Pattern Recognition (CVPR)*, pages 4690–4699, 2019.

[20] Yoshua Bengio, Jérôme Louradour, Ronan Collobert, and Jason Weston. Curriculum learning. In *International Conference on Machine Learning (ICML)*, pages 41–48, 2009.

[21] Lu Jiang, Zhengyuan Zhou, Thomas Leung, Li-Jia Li, and Li Fei-Fei. Mentornet: Learning data-driven curriculum for very deep neural networks on corrupted labels. In *International Conference on Machine Learning (ICML)*, pages 2304–2313. PMLR, 2018.

[22] Tianyi Zhou and Jeff Bilmes. Minimax curriculum learning: Machine teaching with desirable difficulties and scheduled diversity. In *International Conference on Learning Representations (ICLR)*, 2018.

[23] Rajeev Ranjan, Carlos D Castillo, and Rama Chellappa. L2-constrained softmax loss for discriminative face verification. *arXiv preprint arXiv:1703.09507*, 2017.

[24] Ying-Peng Tang and Sheng-Jun Huang. Self-paced active learning: Query the right thing at the right time. In *Proceedings of the AAAI Conference on Artificial Intelligence (AAAI)*, pages 5117–5124, 2019.

[25] Yu-Chi Ho and David L Pepyne. Simple explanation of the no-free-lunch theorem and its implications. *Journal of optimization theory and applications*, 115(3):549–570, 2002.

[26] Jingzhao Zhang, Tianxing He, Suvrit Sra, and Ali Jadbabaie. Why gradient clipping accelerates training: A theoretical justification for adaptivity. In *International Conference on Learning Representations (ICLR)*, 2019.

[27] Yair Carmon, John C Duchi, Oliver Hinder, and Aaron Sidford. Accelerated methods for nonconvex optimization. *SIAM Journal on Optimization*, 28(2):1751–1772, 2018.

[28] Gamaleldin Elsayed, Dilip Krishnan, Hossein Mobahi, Kevin Regan, and Samy Bengio. Large margin deep networks for classification. In *Advances in Neural Information Processing Systems (NeurIPS)*, 2018.

[29] Alexia Jolicoeur-Martineau and Ioannis Mitliagkas. Gradient penalty from a maximum margin perspective. *arXiv preprint arXiv:1910.06922*, 2019.

[30] Kaiming He, Xiangyu Zhang, Shaoqing Ren, and Jian Sun. Deep residual learning for image recognition. In *Proceedings of the IEEE/CVF Conference on Computer Vision and Pattern Recognition (CVPR)*, pages 770–778, 2016.

[31] Karen Simonyan and Andrew Zisserman. Very deep convolutional networks for large-scale image recognition. *arXiv preprint arXiv:1409.1556*, 2014.

[32] Andrew G Howard, Menglong Zhu, Bo Chen, Dmitry Kalenichenko, Weijun Wang, Tobias Weyand, Marco Andreetto, and Hartwig Adam. Mobilenets: Efficient convolutional neural networks for mobile vision applications. *arXiv preprint arXiv:1704.04861*, 2017.

A Appendix

A.1 Implementation details in experiments

In this experiment, we give some other experimental results of a variety of model architectures, such as FCNN, ResNet18, ResNet35, ResNet50 [30], VGG16 [31] and MobileNetV1 [32], trained on MNIST, CIFAR-10/100, SVHN and Tiny-ImageNet. Based on empirical analysis, we briefly show how different β dynamical affect the performance of the models on different datasets.

The shallow three-layer architecture of FCNN with 50, 20 and 10 nodes is implemented on MNSIT. The learning rate is 10^{-3} and weight decay is 10^{-4}. The momentum is set to 0.9. The batch is set to 100 within a total of 100 epochs. $\beta_{initial}$ and β_{end} in the warm-up strategy are set to 0.01 and 0.1, respectively, where over-small $\beta = 0.001$ provides faster convergence in early phase.

The deep models are used for training and predicting in CIFAR-10/100, SVHN and Tiny-ImageNet. The learning rate is 10^{-2} and weight decay is 10^{-4}. The momentum is set to 0.9. The batch is set to 100. CIFAR-10/100 is traversed over 200 epochs, while SVHN is traversed over 100 epochs. At 50% and 75% epochs, the learning rate decreases to 10 percent. At the same time, we set gradient clip with $norm = 3$. For the Tiny-ImageNet, the learning rate was set to 0.05, the batch size to 256, the momentum to 0.9, and the weight clipping to Norm=3. 200 epochs were performed, with the learning rate decreasing to 10% at 40% and 80% epochs, respectively. $\beta_{initial}$ and β_{end} in the warm-up strategy are set to 0.1 and 1, respectively. In real-world training, we find that over-small β may cause the overflow of the Softmax function. So e^z is replaced by e^{z-u} in (21) and u is set to 70 to prevent exp function from being too large in experiments.

$$J = -\log \frac{e^{z_c - u}}{\sum_{i \neq c} e^{z_i - u} + \beta e^{z_c - u}} \tag{21}$$

A.2 Additional results

We can observe that there is a noticeable accuracy oscillation in Fig. 8. In experiments, we find that it is a common phenomenon in different datasets when β is large but this kind of large consolidation does not happen when momentum is small. We attribute this phenomenon to instability resulting from rapid gradient decay in certain samples. To provide a clearer description of this issue, further systematic exposition and experimentation are needed.

In the experiments detailed in Table 4, we investigated the impact of larger gradient decay coefficients on model calibration and generalization in the CIFAR-100. Our findings indicate that as the gradient decay coefficients increase, the overall confidence level decreases, resulting in the model exhibiting underconfidence. Remarkably, despite the model under-confidence, as indicated by the ECE calibration metric, its accuracy continues to improve significantly. This suggests that for CIFAR-100 with ResNet18 and ResNet34 architectures, training consistency between samples is favored.

The results in Fig. 12 and Table 5 demonstrate that smaller gradient decay weights lead to faster convergence speeds, resulting in higher training accuracy. This can be attributed to the imposition of smaller local L constraints by the low

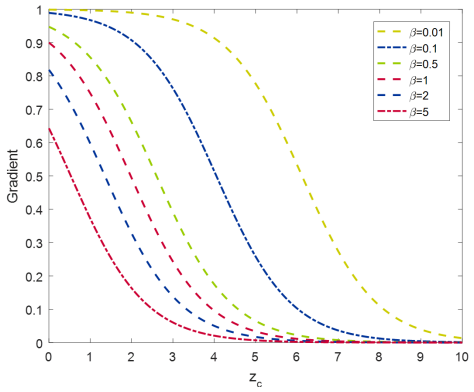


Figure 7: The gradient magnitude as the sample output increases with different hyperparameter values under the assumption: 1) Initialization $z_i = 0, i = 1, \ldots, m$ and $m = 10$ 2) Other class outputs are equal, i.e., $\frac{\partial J}{\partial z_i} = -\frac{1}{m-1}\frac{\partial J}{\partial z_c}, i = 1, \ldots, m, i \neq c$.

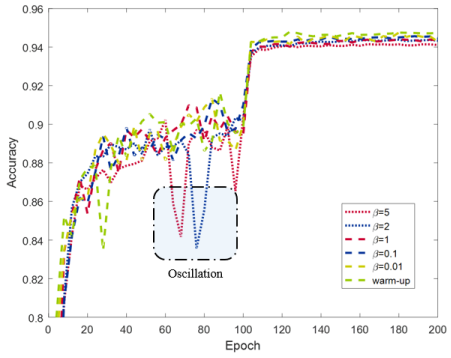


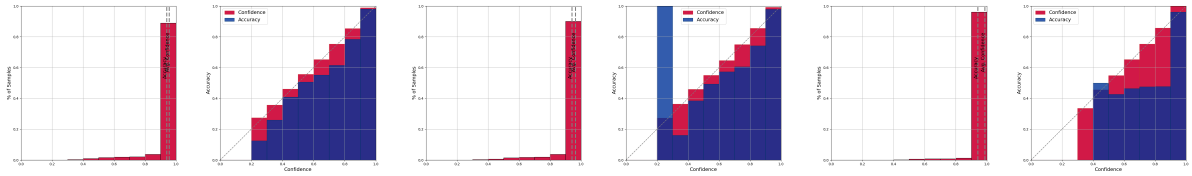
Figure 8: Top-1 accuracy curve on CIFAR-100 with different gradient decay hyperparameters {5, 2, 1, 0.1, 0.01} and warm-up strategy.

Table 4: Top-1 Acc (%), ECE and MCE ($bins = 10$) on CIFAR-100 with ResNet17 and ResNet34

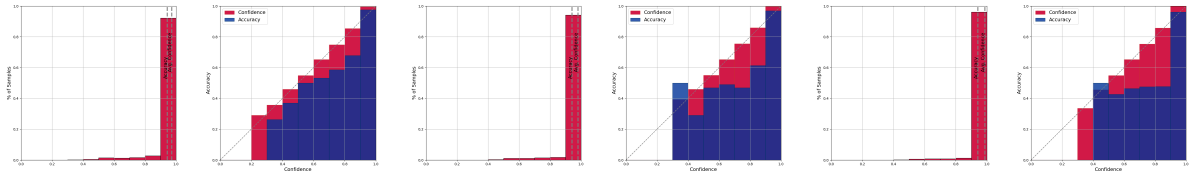
Dataset	Model	Metric	Gradient decay factor β					
			50	20	10	5	1	0.1
CIFAR-100	ResNet18	Top-1 Acc	**75.0**	74.5	74.2	74.1	73.5	73.2
		ECE	0.027	**0.021**	0.059	0.082	0.130	0.181
		MCE	0.141	**0.071**	0.135	0.182	0.298	0.464
CIFAR-100	ResNet34	Top-1 Acc	**75.6**	75.2	74.8	74.5	74.0	73.8
		ECE	**0.024**	0.030	0.065	0.085	0.125	0.170
		MCE	**0.056**	0.091	0.157	0.172	0.273	0.388

Table 5: The performance of ResNet34 on Tiny-ImageNet with different gradient decay.

Metric	Gradient decay factor β					
	20	10	5	1	0.1	0.01
Top-1 Acc (%)	52.8	53.2	**53.8**	53.4	53.7	53.6
Top-5 Acc (%)	**75.8**	75.5	75.1	75.0	74.4	73.2
Training Acc (%)	88.6	88.5	89.7	90.3	**90.9**	90.5
ECE ($bins = 10$)	**0.015**	0.034	0.076	0.087	0.224	0.274
MCE ($bins = 10$)	**0.036**	0.065	0.151	0.176	0.406	0.518

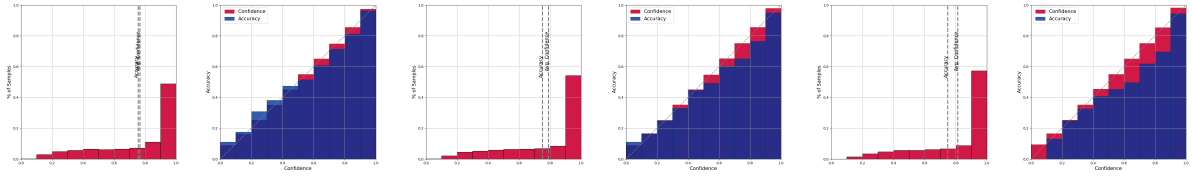


(a) $\beta = 50$ (b) $\beta = 20$ (c) $\beta = 10$

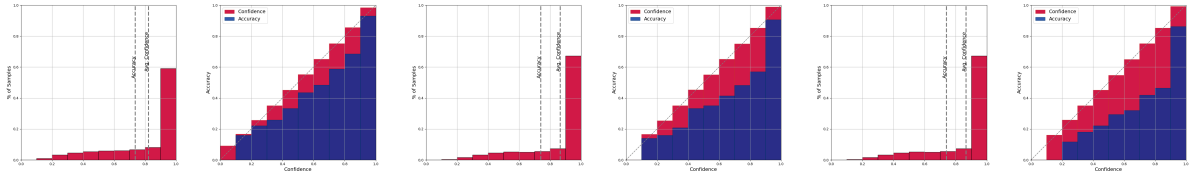


(d) $\beta = 5$ (e) $\beta = 1$ (f) $\beta = 0.1$

Figure 9: Confidence histograms and reliability diagrams for gradient decay with ResNet18 on CIFAR-10. ($bins = 10$)



(a) $\beta = 50$ (b) $\beta = 20$ (c) $\beta = 10$



(d) $\beta = 5$ (e) $\beta = 1$ (f) $\beta = 0.1$

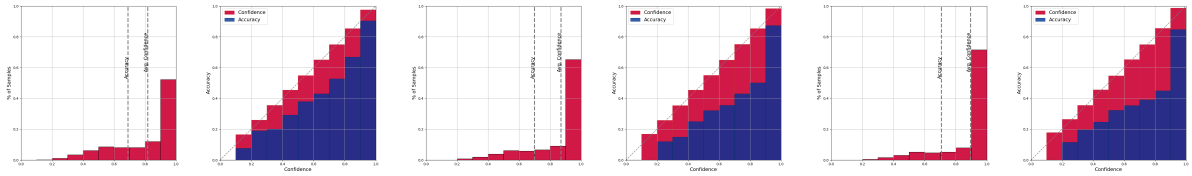
Figure 10: Confidence histograms and reliability diagrams for gradient decay with ResNet34 on CIFAR-100. ($bins = 10$)

gradient decay rate, which in turn increases gradient magnitude. On the other hand, higher gradient decay rates promote optimization consistency and yield better values for metrics such as ECE, MCE, and Top-5 Accuracy. However, these higher gradient decay rates, characterized by smaller gradient magnitudes, do not necessarily lead to improved Top-1 accuracy. Figs. 9-12 consistently demonstrate that larger gradient decay rates lead to improved model confidence.

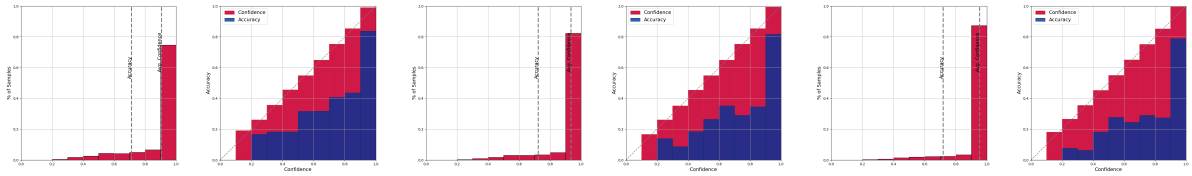
A.3 Discussion

The penalization of larger margin Softmax leads to a deceleration in the gradient decay rate, which exerts influence on amples throughout the dynamics training process. Smaller gradient decay enforce a stricter curriculum learning sequence, thereby augmenting the confidence of easier samples. Conversely, challenging samples are more susceptible to being overlooked due to the learning sequence, ultimately culminating in poor model calibration.

In all experiments, despite the consistent application of an identical learning rate to control the scalar method and draw scientifically grounded conclusions, we inadvertently neglected to consider the impact of varying gradient magnitudes in the learning process. As illustrated in Table 2, a high gradient decay rate may yield insufficient learning outcomes for certain samples, resulting in undesirable performance. In essence, the gradient decay rate not only impacts the learning sequence among individual samples but also influences the gradient magnitude concerning the overall sample learning

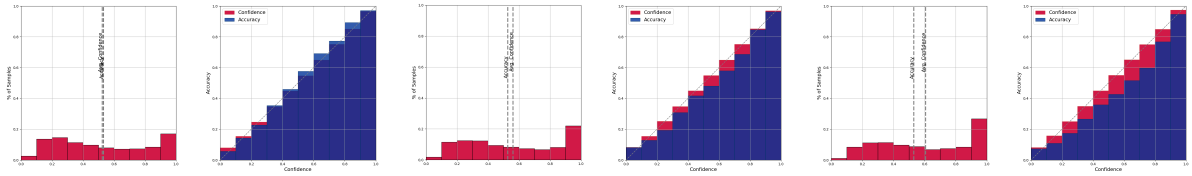


(a) $\beta = 50$ (b) $\beta = 20$ (c) $\beta = 10$

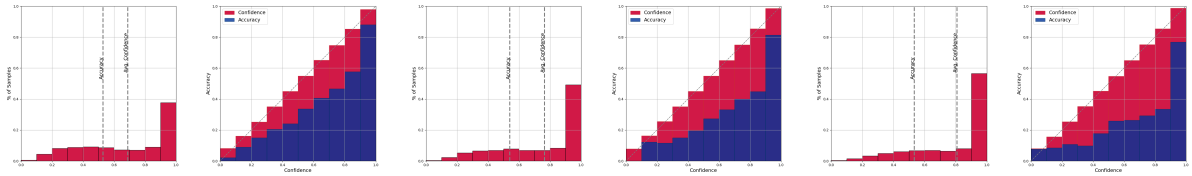


(d) $\beta = 5$ (e) $\beta = 1$ (f) $\beta = 0.1$

Figure 11: Confidence histograms and reliability diagrams for gradient decay with VGG16 on CIFAR-100. ($bins = 10$)



(a) $\beta = 20$ (b) $\beta = 10$ (c) $\beta = 5$



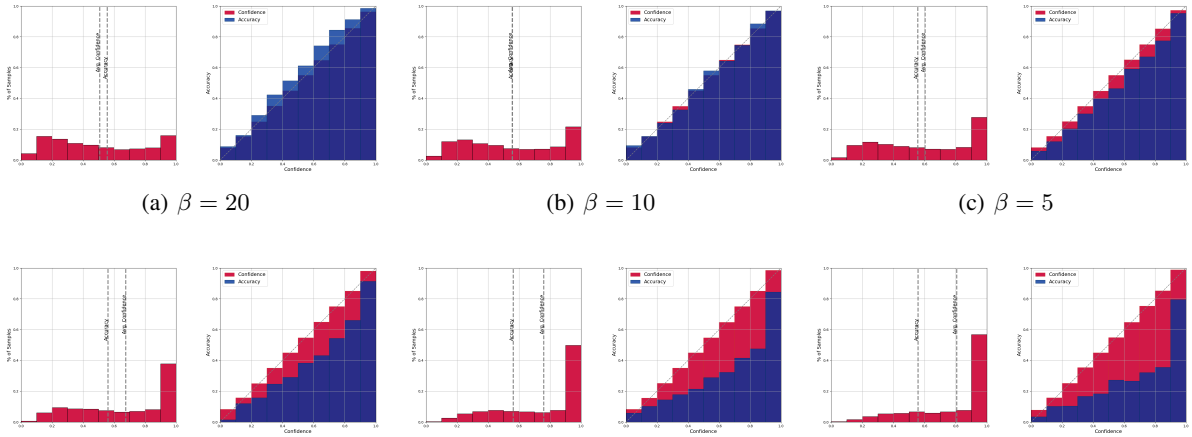
(d) $\beta = 1$ (e) $\beta = 0.1$ (f) $\beta = 0.01$

Figure 12: Confidence histograms and reliability diagrams for gradient decay with ResNet34 on Tiny-ImageNet. ($bins = 10$)

process. To attain more scientifically robust conclusions, it becomes imperative to employ more meticulously designed experiments and generate corroborating results.

As such, one potential direction for future research is to employ more rigorously designed experiments to probe into the dynamic properties of gradient decay coefficients during the optimization process. Expanding on the previous discussion, there is a promising avenue for technical improvement related to designing decay coefficients or incorporating adaptive mechanisms during training. Besides, a high gradient decay rate can result in an overall gradient that becomes excessively small, thereby hindering the training process. Developing methods specifically designed to adjust learning rates based on gradient decay coefficients holds the potential to significantly enhance the efficiency of model training procedures. It ultimately enables the modification of the learning rate scheduler to achieve effective model calibration with the large gradient decay and to prevent under-training due to small gradients.

Furthermore, we posit that the distinct patterns exhibited by varying gradient decay coefficients across different experiments are closely linked to the model's capacity and the dataset's level of complexity. These conclusions warrant a more systematic and rigorous discussion.



(a) $\beta = 20$ (b) $\beta = 10$ (c) $\beta = 5$

(d) $\beta = 1$ (e) $\beta = 0.1$ (f) $\beta = 0.01$

Figure 13: Confidence histograms and reliability diagrams for gradient decay with ResNet50 on Tiny-ImageNet. ($bins = 10$)

Table 6: The performance of ResNet50 on Tiny-ImageNet with different gradient decay.

Metric	Gradient decay factor β					
	20	10	5	1	0.1	0.01
Top-1 Acc (%)	55.9	56.0	**56.4**	56.3	56.4	56.2
Top-5 Acc (%)	77.7	**78.0**	77.3	76.6	76.0	74.9
Training Acc (%)	86.4	88.8	90.3	91.9	**92.3**	91.8
ECE ($bins = 10$)	0.045	**0.014**	0.046	0.114	0.203	0.249
MCE ($bins = 10$)	0.084	**0.044**	0.082	0.151	0.388	0.476